Effect of the cap layer growth temperature on the Sb distribution in InAs/InSb/InAs sub-monolayer heterostructures for mid-infrared devices

Atif A Khan[1], E Repiso[2], M Herrera[1], P J Carrington[3], M de la Mata[1], J Pizarro[4], A Krier[2], S I Molina[1]

[1] Department of Material Science, Metallurgical Chemistry and Inorganic Chemistry, IMEYMAT, University of Cádiz, 11510 Puerto Real, Spain.

[2] Physics Department, Lancaster University, Lancaster, LA1 4YB, UK

[3] Engineering Department, Lancaster University, Lancaster, LA1 4YW, UK

[4] Department of Computer Engineering, ESI, University of Cádiz, 11510 Puerto Real, Spain.

Abstract

Sub-monolayer (SML) deposition of InSb within InAs matrix by migration enhanced epitaxy (MEE) tends to form type II SML nanostructures offering efficient light emission within the mid-infrared (MIR) range between 3-5 µm. In this work, we report on the Sb distribution in InSb/InAs SML nanostructures with InAs cap layers grown at temperatures lower than that associated with the under-grown InSb active layer. Analysis by transmission electron microscopy (TEM) in 002 dark field (DF) conditions shows that the reduction in the growth temperature of the InAs cap layer increases the amount of Sb deposited in the layers, in good agreement with the X-ray diffraction (XRD) results. TEM micrographs also show that the layers are formed by random InSbAs agglomerates, where the lower cap temperature leads to a more continuous InSb layer. Quantitative atomic column resolved high angle annular dark field (HAADF)-scanning (S)TEM analyses also reveal atomic columns with larger composition of Sb for the structure with the lowest InAs cap layer temperature. The dependence of the Sb distribution on InAs cap growth temperature allows tuning the corresponding emission wavelength in the MIR range, as shown by the photoluminescence (PL) emission spectra.

Keywords: InSb/InAs sub-monolayer nanostructures, 002 Dark Field analysis, Atomic column HAADF-(S)TEM, Sb segregation, Composition analysis

Introduction

Previous reports on the epitaxial growth of sub-monolayer (SML) quantum dots (QDs) indicate increased dot density, quantum confinement and size uniformity with smaller base diameter [1,2] than its Stranski-Krastanow (SK) [3] counterpart which is the typical III-V epitaxial QD formation method [4]. III-V SML QDs are formed due to SML, i.e., ~ 1 ML epitaxial deposition of a III-V binary in solo or in stacks into another type of III-V barrier material(s) [5-12]. The deposition of these SML insertions into the barrier layers is often carried out using the migration enhanced epitaxy (MEE) technique [7, 13, 14], where the atomic species of the III-V sub-lattices are alternatively supplied to the surface instead of the simultaneous deposition of the conventional epitaxy (CE) growth mode. It is claimed that such deposition technique could avoid the formation of the wetting layer (WL) intrinsic to the SK growth mode. In this case, no carrier scattering would occur between the WL and the QDs leading to the enhancement of the

associated modulation bandwidth (BW) and maximum gain [12]. SML QDs have been used to design various kinds of optoelectronic devices, such as- lasers [15, 16], virtual-cavity surface-emitting lasers (VCSELs) [17], photo-detectors (PDs) [18], solar cells (SCs) [19], etc.

In particular, SML heterostructures based on InSb/InAs are an attractive option for achieving efficient mid-infrared (MIR) emission in the 2 or 3-5 µm spectral region used for light emitting diodes (LEDs) [6, 20] and lasers [5, 7]. The type II broken gap band alignment leads to strong hole localization within the InSb SML whilst electrons are loosely confined within the InAs matrix. This leads to a reduction in non-radiative Auger recombination leading to an increase in the radiative efficiency. Therefore, InSb/InAs SML insertions have been reported to exhibit intense MIR photoluminescence (PL) up to room temperature [6]. The emission wavelength of these heterostructures can be tuned by modifying the nominal thickness of the InSb insertions, through the control of the growth temperature [5]. In this sense, growth temperatures of the InSb insertions in the range 400ºC-485ºC have been found to provide emission in the MIR regime [5].

However, recently we have demonstrated by TEM techniques that the growth of InSb/InAs SML heterostructures by MEE at 430ºC forms an inhomogeneous InSbAs layer with a thickness of ~ 3 nm that contains InSbAs agglomerates with low Sb composition (~5-10%) [21]. The formation of this relatively thick layer is somewhat compatible with the strong tendency of Sb to segregate upwards during growth [22], supported by the corresponding large segregation coefficient measured from the composition profile. In GaSb/GaAs quantum rings, the strong Sb segregation observed has been related to an extensive group-V atomic exchange, in this case As/Sb exchange, during the growth of the capping layer on the nanostructures [23]. These group V exchange reactions can even modify significantly the morphology of InGaSb/GaAs QDs grown by MEE [24]. In this instance, it has been found that reducing the growth temperature of the GaAs cap (known as cold capping technique) helps to preserve the QD morphology during MEE growth [24]. For conventional InSb/InAs SK QDs grown by MEE, Zhuang *et. al.* [25] reported that a reduction of the InAs barrier layer growth temperature (regarding the InSb temperature) dramatically improved the emission efficiency, associated with a reduction in the As/Sb exchange. Inspired by this outcome, in this work we investigate the formation of InSb/InAs SML QDs heterostructures with InAs cap layers grown at temperatures lower than that used to obtain the InSb SML insertions (380ºC and 310ºC for the InAs capping layers, 430ºC for the InSb). The effect of the cap temperature on the Sb distribution and on the PL emission is discussed.

Materials and methods

Two InSb/InAs heterostructures have been grown by MEE on n-InAs substrates with different InAs cap temperatures. Each sample has three InSb layers. Initially, a 500 nm InAs buffer layer is grown on the InAs substrate at 470ºC. Then, 20 nm of InAs is deposited at a growth temperature of 430ºC. For the deposition of each InSb layer, the InAs surface is exposed to an Sb_2 flux for 20s, then pure In for 5s and again Sb_2 for 6s while maintaining a growth temperature of 430ºC. Afterwards, the growth is interrupted and the temperature lowered to the desired cap temperature under a Sb_2 flux. The InSb SMLs are capped with 13 nm of InAs, at temperatures of 380ºC and 310ºC for the two samples considered. Due to the lower growth temperature for the InAs cap, they are called cold caps (CCs). The temperature is then increased to 470ºC to grow a 33 nm InAs layer, followed by another 20 nm of InAs layer grown at 430ºC, and then the next InSb layer is grown with a similar procedure. This implies that the active layer

periodicity of the CC samples is ~ 66 nm. Finally, an InAs layer of 100 nm is grown at 470°C. An additional sample where the InAs cap layer is grown at the same growth temperature of the InAs layers (which is the conventional procedure) although containing 10 InSb layers instead of 3 with active layer periodicity of ~ 20 nm is also considered for comparison. The growth of the layers was monitored using *in situ* reflection high energy electron diffraction (RHEED) and the corresponding growth temperature T_s was measured by calibrated thermocouple.

Low temperature (4K) photoluminescence (PL) has been performed on the samples using a single mode laser diode with an emission wavelength of 785 nm and a 1mm^2 spot size that leads to a power density of 20W/cm^2. For XRD analyses, ω-2θ symmetric scans were performed using a Bede QC200 double crystal machine. The nominal thickness of the InSb layer and corresponding structural period was obtained from the XRD simulation using RADS Mercury software.

A combination of mechanical thinning and precision ion polishing system (PIPS) associated Ar$^+$ ion milling was used to prepare the electron transparent specimens for the TEM analyses. The diffraction contrast analysis was carried out using a JEOL JEM 2100 microscope at an operating voltage of 200 kV. A double aberration corrected FEI Titan Cubed Themis microscope was used for atomic column resolved high angle annular dark field (HAADF)-scanning TEM ((S)TEM) analysis of the specimens at 200 kV. The imaging parameters used to acquire corresponding HAADF-(S)TEM images are: $C_s = 1$ μm, $C_5 = 5$ mm, HAADF detector inner angle = 63.8 mrad, convergence angle = 16.04 mrad and camera length = 91 mm. The HAADF-(S)TEM images were taken from regions of the specimens that possess an average relative log-ratio value of $t/\lambda \sim 0.41$ and 0.47 for specimens with 380°C and 310°C CCs, respectively, measured using zero-loss peak electron energy loss spectroscopy (EELS). Here, 't' represents the thickness of a region, while 'λ' denotes the corresponding electron mean free path (MFP). The MFP with the value of ~ 62.14 nm was found in both cases, calculated using the method by Malis *et. al.* [26].

Results and discussion

Figure 1 shows the low temperature (4K) normalized PL profiles in red and green associated with the samples of InAs CC grown at 380°C and 310°C, respectively. The PL profile of the structure with the InAs cap grown at 430°C has also been included for comparison (in black). As it can be observed, the InAs peak is located at a wavelength of ~ 3 μm in all samples, similar to the InAs induced PL responses observed in refs. [5-7, 25]. There is a small shifting between the InAs peaks from 380°C and 310°C/430°C samples. The InAs PL emission originates from near band edge states including shallow donors and acceptors. The origin of the small shift observed could be related to the 380°C sample containing more of these impurities or being of lower crystalline perfection (since linewidth is also a bit larger). Lower PL powers have been also used to look for excitons but none could be identified. On the other hand, it can be observed that although the InAs intensity is reduced in the 430°C sample, the linewidth of the InAs related PL remains narrow, which indicates good crystalline quality. This lower intensity from the InAs most probably originates from non-radiative (surface) recombination in the upper 100nm InAs upper layer or the InAs buffer. To clarify how much the emission levels of InSb and InAs vary in a sample, we have included the corresponding non-normalized PL spectra of each sample as an inset in the normalized PL spectra in Figure 1. However, we must note that it is unreliable to compare absolute PL intensities due to alignment factors, etc. The non-normalized PL intensity of the InSb grown at 430°C is the highest consistent with good crystalline quality in these nanostructures. It should also be noted that the PL

intensity dips at ~ 4.2 μm in all samples are due to the presence of CO_2 absorption from the atmosphere during PL measurements [6]. In addition, the feature around 2.75 μm in the PL spectrum is due to an instrumental artifact arising from imperfect cancellation of the background in the Fourier-transform infrared (FTIR) spectrometer. This happens at this wavelength due to the atmospheric water vapor absorption near 2.7 μm.

Regarding the normalized InSb signal, it can be seen that the sample with CC grown at the conventional growth temperature of 430ºC (black line) exhibits one PL peak, at a wavelength of ~ 4 μm. When the InAs CC growth temperature is reduced to 380º C (red line), the PL emission changes, and two InSb peaks at 3.7 μm and 4.6 μm, respectively, are found. The reasons behind the differences observed in the PL spectra are likely related to a difference in the Sb distribution in the material. The two InSb peaks at different wavelengths observed in the sample with 380ºC InAs CC could be due to the formation of two distinct quantum structures within the InSb layer regions. Semenov *et al.* [27] demonstrated two InSb PL peaks originated by high excitation power density at 110K in InSb/InAs SML nanostructures, claiming that these peaks appear due to the presence of both InSb QDs and a InAsSb WL in the material. In our case, the peaks observed could be related to regions of the InSb layer with different morphology and/or Sb content. In comparison to the sample with InAs cap grown at 430ºC, the PL peaks observed appear one at longer wavelength and one at a shorter wavelength than the ~ 4 μm peak of the sample 430ºC. This suggests that upon reducing the InAs CC growth temperature, some regions of the InSb layer become richer in Sb, leaving other regions with less Sb content. This could point to the formation of initial Sb clusters or QDs with a density significant enough to produce a remarkable variation in the PL emission. When further reducing the InAs CC growth temperature to 310ºC, Fig. 1 shows that only one PL peak at the longer wavelength of 4.6 μm is observed. It is well known that the incorporation of Sb in III-V semiconductors reduces the corresponding bandgap energy and hence, induces a red shift in wavelength [28, 29], where a higher Sb composition imposes a larger red shift [6]. This suggests the existence of one type of quantum structure with a larger Sb content in this heterostructure. In order to investigate the aforementioned assumptions, post-growth X-ray diffraction (XRD) measurements and 002 dark field (DF) TEM analyses of these samples have been performed.
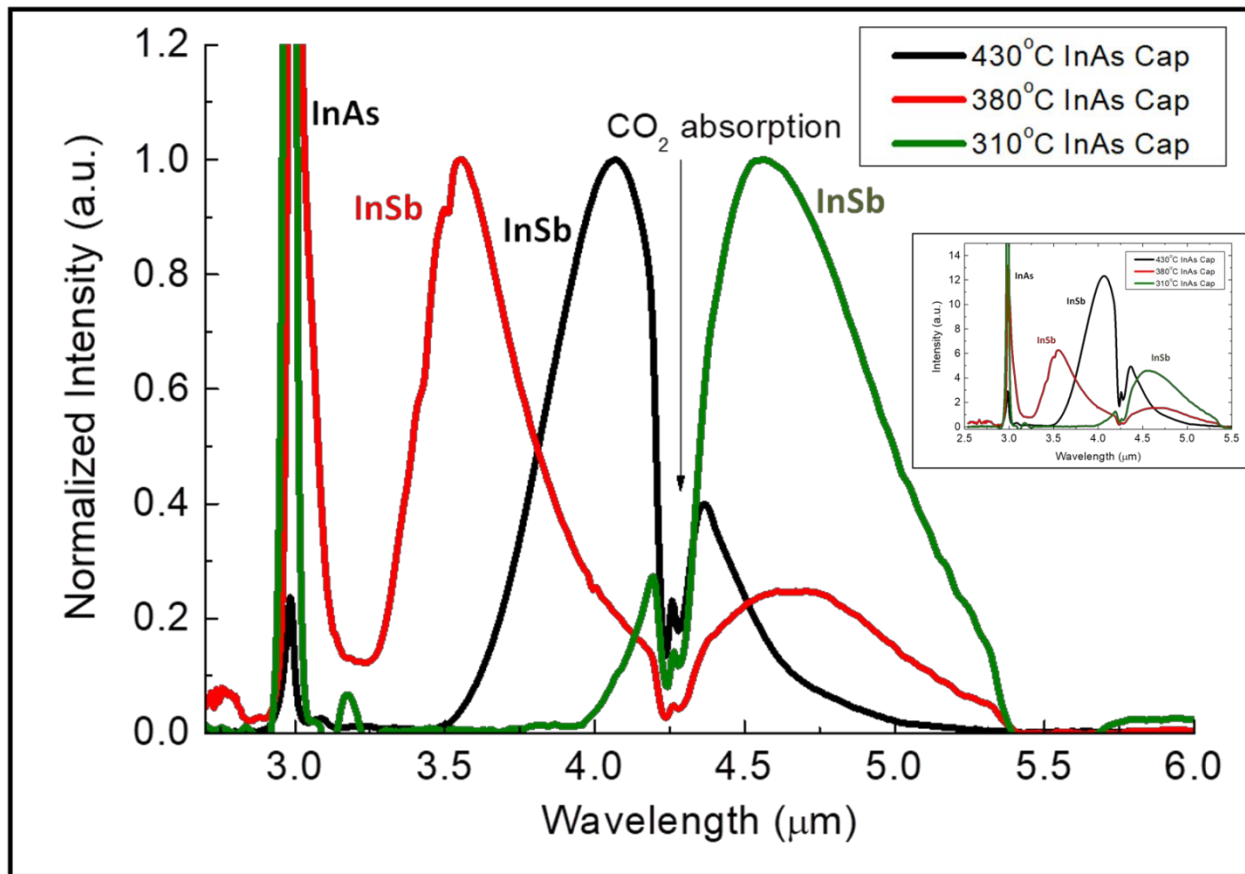
Figure 1: Normalized PL response (4K) associated with 430ºC, 380ºC and 310ºC InAs cap samples in black, red and green, respectively. The inset represents the non-normalized version of the PL spectra.

Figure 2a shows the post-growth XRD profiles obtained from the samples with InAs CCs grown at 380ºC (black line) and at 310ºC (red line), respectively. The XRD profile of the structure with the InAs cap layer grown at 430ºC has also been included for comparison (blue line). In each profile, the highest peak represents the Bragg diffraction from the InAs substrate and the satellite peaks specify the corresponding Bragg diffractions associated with the overgrown InSb layers. It should be noted that the active layer periodicity of the reference sample is different from the CC samples, as mentioned before. In the insets, sample-specific individual experimental XRD spectra together with the corresponding simulated XRD curves are included. It should be highlighted that some disagreements regarding the active layer periodicity between the XRD simulations and the experimental growth structure is observed. This disagreement could be due to the limited modeling capability of XRD, which does not take into account the sticking coefficients of In and As_2, possible Sb segregation, group V atomic exchange, graded InSbAs barriers, change in growth rate over the associated temperature range, etc. It is not easy to determine the exact reason from the discrepancy as there may be a wide variety of parameters involved. As it can be observed in Figure 2a, the satellite peaks corresponding to the 430ºC InAs cap sample (in blue) appear at a larger distance from one another compared to the satellite peaks obtained from 380ºC (in black) and 310ºC (in red) InAs CC samples. These last two samples have only a slight shift between some satellite peaks, where one of these shifts is indicated by a blue arrow in Figure 2a. However, it must be noted that in thicker layers, thickness variations between layers provide smaller differences in the XRD profiles that

in thin layers. Assuming flat layers of pure InSb composition, a higher separation between two consecutive satellite peaks (in Figure 2a), induced by active region periodicity denotes a lower overgrown InSb layer thickness and vice versa (a nice review on XRD can be found in ref. [30]). Therefore, the observed XRD profiles indicate that the growth temperature of the InAs caps in these structures may affect the thickness and/or the morphology of the InSb layers. With the abovementioned assumptions, thicknesses of 0.65 ML, 0.86 ML and 1.02 ML have been calculated for InAs cap growth temperatures of 430ºC, 380ºC and 310ºC, respectively. This suggests an increase in the incorporation of Sb for reduced InAs CCs growth temperatures. The XRD results are consistent with the PL results which showed a larger emission wavelength associated with a larger Sb composition in the 310ºC sample. However, it should be noted that different Sb distributions could also account for the XRD results obtained, as 3D In(As)Sb complex nanostructures are likely to have formed during the growth. In order to obtain direct compositional information on the Sb distribution in the material, the samples have been analyzed using TEM techniques.

Figures 2c and 2d show diffraction contrast images of the samples with InAs CCs grown at 380ºC and 310ºC, respectively, obtained in 002 DF conditions. For comparison, Figure 2b includes an image of the sample with the InAs cap grown at 430ºC, where the conventional approach of growing both InSb and InAs cap layers at the same temperature was followed. All 002 DF images in Figure 2b-2d are shown in temperature color grade to induce better graphical representations as per chemical contrast based intensity variations in arbitrary units (a.u.). In each image there is a central low intensity area in green/blue that corresponds to the InSb region, sandwiched between high intensity InAs cap and barrier layers. It should be noted that some intensity variability is observed in the homogeneous InAs barrier layers, due to small specimen thickness fluctuations related to the TEM specimen thinning process to electron-transparency. A comparison of Figures 2b, 2c and 2d reveals that the Sb containing layer is thicker and has smaller intensity for reduced InAs CC growth temperature. This is consistent with a larger incorporation of Sb in the material for reduced temperatures (380ºC and 310ºC), supporting the XRD results obtained above. In InAs/InAsSb type-II superlattices (SLs) grown on GaSb by MBE, an increase in the Sb incorporation in the InAsSb layers has been reported when the SL growth temperature is reduced [22, 31]. The authors attribute their finding to the preferential incorporation of Sb in InAsSb at lower temperature. Our results suggest that not only the growth conditions of the Sb-containing layer have a strong impact on Sb incorporation, but also the parameters used for capping such active layers.

A detailed observation of the 002 DF images obtained shows that the InSb distribution in the layers is not regular, forming random nucleated regions (in blue) along the layers. These Sb agglomerations do not show shapes that could be clearly identified as any common QD shape reported in the literature (cuboid, cylindrical, pyramidal, etc. [32]). Some agglomerates with height clearly larger than the layer beside them can be observed in the sample with the InAs cap grown at 430ºC, as shown by the white arrows in Figure 2b. This holds true for the structure with InAs CC grown at 380ºC, where a clear agglomeration is marked by the white arrow in Figure 2c, although in this case it seems to be embedded into the InSbAs layer. However, in the InSb/InAs heterostructure with InAs CC grown at 310ºC in Figure 2d, there seems to be a thicker and more continuous layer, rather than isolated agglomerates. In this sense, the red-shift observed in the PL emission of these samples when the InAs CC growth temperature is reduced can be justified by the increase in the Sb content derived from the 002 DF images. The PL spectra for the sample with InAs CC at 380ºC show two peaks at different wavelengths. This means that two different quantum structures with statistical significance should be present in the material, although these quantum structures

are not obvious from the corresponding TEM image in Figure 2c. TEM analyses allow studying small regions of the material of interest, normally of several tens of nm. On the other hand, PL analysis provides information related to comparatively larger regions, up to several hundreds of nm. Because of this, sometimes a direct correlation between the results obtained by these techniques is difficult to carry out. On the other hand, the single peak observed at longer wavelength in the sample with InAs CC at 310ºC could be associated with the Sb-rich continuous layer observed (or bigger Sb agglomerates). The single PL peak observed for the sample with the InAs cap obtained at 430ºC could be related to the small agglomerations found in 002 DF. In order to obtain further information on the Sb distribution in the materials with higher spatial resolution and to quantify the Sb content in the layers, the samples were analyzed by aberration corrected atomic column HAADF-(S)TEM.
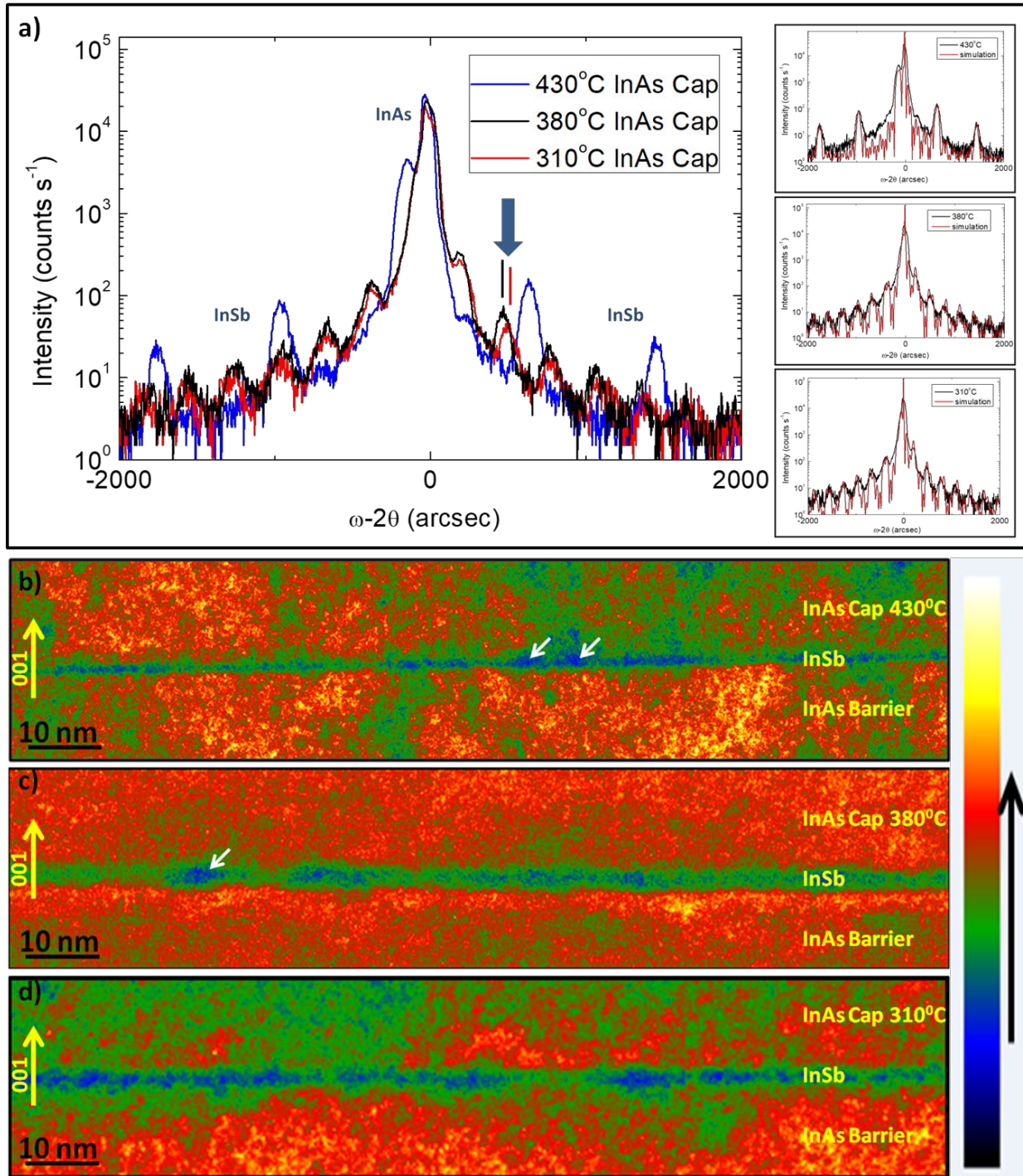
Figure 2: (a) XRD spectra from the three InSb/InAs samples which contain InAs caps grown at 430ºC, 380ºC and 310ºC, denoted by blue, black and red lines, respectively. The insets represent sample-specific individual experimental XRD spectra from Figure 2a and their corresponding simulated XRD curves. Temperature graded 002 DF TEM images of single InAs/InSb/InAs layers taken from samples with InAs cap growth temperatures of (b) 430ºC, (c) 380ºC and (d) 310ºC, illustrating intensity variations within the heterostructures. The color scale demonstrates increase in intensity from black to white (in a.u).

Figures 3a and 3b exhibit HAADF-(S)TEM images showing a single InAs/InSb/InAs layer of the samples with 380ºC and 310ºC InAs CC, respectively. In these images, microscope induced vacuum signal has been subtracted using the approach illustrated in ref. [33], as it is a requirement for precise quantitative HAADF-(S)TEM analysis.In both samples a layer where the HAADF-(S)TEM intensity is larger than the region above and below it can be observed at the center of the image. As in HAADF-(S)TEM images the intensity is roughly proportional to the square of the average atomic number in the material ($Z^{\sim 1.7-2}$), the observed layers can be associated with the Sb-containing layers. These high intensity dumbbells appear to be forming single thin layers in each image, along with few agglomerates. In order to obtain a clearer picture of the Sb distribution in each heterostructure, we have quantified the Sb composition with atomic column resolution. For this, initially we used the quantitative HAADF (qHAADF) tool, developed by Molina *et. al.* [34]. This tool compares atomic column-by-column intensities from a region of interest (ROI) with the average atomic column intensity from a homogeneous material region (reference) in a single HAADF-(S)TEM image and reveals atomic column-by-column normalized integrated intensity, R' on the ROI. Afterwards, these R' values are converted to atomic column-by-column Sb composition (in %) using the method by Maldonado *et. al.* [35]. However, it should be mentioned that the HAADF-(S)TEM intensity is not only related to the average Z number in the material, as the thickness of the specimen (thin foils) used for the analysis also have an important effect. As shown in ref [36], a precise estimation of the composition from HAADF-(S)TEM images using the method explained above requires that both ROI and reference regions have the same thickness. Because of that, simultaneous zero-loss peak EELS analysis was performed during the acquisition of each HAADF-(S)TEM image in order to measure specimen thickness. This analysis revealed an average thickness variation between ROI and reference regions in either image to be < 1 nm. Although this average thickness variation is quite low, its compensation allows more precise Sb induced R' values to be obtained. According to the simulated images induced R' vs ROI-reference specimen thickness variation profiles in ref. [36], we have introduced an additional parameter of $\pm$ 0.02*Δt, where Δt represents specimen thickness variation between ROI and reference regions in nm, to the qHAADF formula in ref. [34] that allows calculating the corrected R' values. The composition values obtained with these corrected R' values using the approach by Maldonado *et. al.* [35] are illustrated in the insets of Figure 3a and 3b as color maps. In particular, those maps correspond to the Sb agglomerates within a yellow rectangle in the respective image (ROI areas) whereas the reference areas are located in the InAs barrier layers, marked with green rectangles. These Sb composition color maps demonstrate that Sb is distributed within few atomic columns in the agglomerates. No uniform and defined shape has been found among the different agglomerates analyzed. In order to evaluate possible differences in the Sb content in these structures with InAs CC grown at different temperatures, we performed a statistical analysis on the atomic column composition using several images from either sample and represented the corresponding data in a histogram illustrated in Figure 3c. In this Figure, the black and red bars correspond to the results obtained for the 380ºC and 310ºC CC samples, respectively. It should be noted that the region of the material analyzed when a sample is studied by atomic column (S)TEM techniques is very small, typically several tens of nms, so care should be taken in the quantitative interpretation of statistical data , because the data may vary slightly when moving to another region of the material. The sample with the 310ºC InAs CC has a larger number of atomic columns with Sb composition in the range 21-30% Sb, whereas the structure with the 380º InAs CC has them in the range 11-20 %. In a previous paper [21], we quantified by TEM techniques the Sb content in the structure with an InAs cap layer obtained at 430ºC, and found that the InSb layer had

Sb content of ≤ 10%. Thus, our results show a clear increase in the Sb content in the InSb layer for reduced InAs CC growth temperatures.

The analysis of the sample with the InAs cap layer grown at the same temperature of 430ºC as the undergrown InSb layer in the conventional manner published previously by the authors showed a strong Sb segregation during growth [21]. This segregation could be partly responsible for the differences in the Sb distribution in the samples with different InAs CC growth temperature observed in this work. In order to investigate the Sb segregation for the lower InAs CC growth temperature of 310ºC considered in this work, the ML-by-ML average Sb composition profile (in black) as per the composition map in Figure 3b is shown in Figure 3d., The maximum average Sb composition in a ML within the analyzing region has been found to be 24%, and the composition profile shows asymmetric edges along the growth direction: the interface between the InAs cap layer and the InSb layer is more graded than the interface between the InSb layer and the undergrown InAs barrier. This is the typical profile of an interface with upwards segregation during growth. In order to quantify the Sb segregation coefficient, the theoretical Muraki segregation model [37] has been considered. This model has been successfully implemented to analyze Sb segregation in InAs/InAs$_{1-x}$Sb$_x$ type-II superlattices [38], GaInSb/InAs strained-layer superlattices [39], etc. To perform Sb segregation analysis in terms of Sb composition in Figure 3d, the maximum Sb compositions must be positioned at ML1 and so on and so forth in either case as per model requirement. The formulation used for this quantification is as follows:

$$x = x_0 \, (1 - R^N) \, R^{z-N}, \text{ for } z \geq N$$

Here, x is the average ML-by-ML Sb composition, x_0 is the nominal InSb composition, z is the number of analyzing MLs at ML≥0, R is the segregation coefficient and N is the nominal thickness of the InSb layer.

The Muraki model fit obtained is demonstrated by a red profile (in %) in Figure 3. Local deviations of the composition values in the experimental profile regarding the theoretical model can be observed. These local fluctuations are unavoidable when composition values obtained with very high spatial resolution and from a very small region of the material are considered. In this case, due to the small size of the clusters, averaging the data over larger areas is not possible. Despite this, the authors believe the fitting of the experimental data to the theoretical model is reasonably good enough to obtain an estimation of the segregation coefficient in the material. The best Muraki fit has been obtained with an R of 0.61 for a nominal InSb deposition thickness of 1.09 ML which is in good agreement with the deposition thickness of 1.02 ML obtained in the XRD analysis. Semenov *et. at.* [27] estimated by RHEED the Sb segregation coefficient in InSb/InAs SML insertions for different InSb growth temperatures in the range 410ºC-500ºC, finding a linear reduction of this coefficient with temperature. If their data is extrapolated to the growth temperature of 310ºC, a value of R of 0.59 is obtained, which is in a good agreement with the value obtained in the present work. This segregation coefficient is smaller than the segregation coefficient of 0.81 obtained using the same procedure by the authors in the sample with InAs cap growth temperature of 430ºC in a previous paper [21], indicating that the reduction in the InAs CC growth temperature has a direct effect on the Sb segregation during growth.

The results obtained by XRD and (S)TEM in the present work have shown an increase in the Sb content in SML InSb/InAs heterostructures when the growth temperature of the InAs cap layer is reduced. In relation to this, in superlattices of Sb MLs in (InGaAl)As grown by MEE, an increase in the amount of Sb incorporated in the material when decreasing the superlattice growth temperature has been found by XRD

[40]. In particular, for Sb MLs in InAs, this has been found to occur in the temperature range 465-400ºC, and it is observed that the growth temperature should be less than 420 °C to achieve a complete ML of InSb per period. The authors claim that their results are consistent with Sb evaporation at higher temperatures, and relate their finding with the congruent sublimation temperature of the binaries (400 °C for InSb). Haugan *et. al.* [22] found that in InAs/InAsSb superlattices, the Sb content increased by 14% as the growth temperature decreased from 440 to 400 ºC, and attributed their finding to Sb surface segregation during InAsSb growth through the As-Sb exchange process. The effect of the InAs cap growth temperature on the Sb incorporation in InAs reported in the present work is in line with the effect of the InSb SL growth temperature, as the reduction of both seems to improve the Sb incorporation. Here, it has been possible to introduce a complete InSb ML in InAs at high growth temperatures (430ºC), by reducing the InAs CC temperature to 310ºC. Thus, our results highlight the importance of the cap layer growth conditions on the characteristics of the InSb layers obtained. The increase in the Sb content in the InSb layers analyzed could be due to two different phenomena. On the one side, our results have shown a clear decrease in the Sb segregation coefficient when reducing the CC growth temperature. In relation to this, the success of the MEE technique for the growth of InSb SML nanostructures is attributed to a very efficient Sb/As anion exchange reaction that occurs upon exposure of the InAs surface to the Sb flux [7], also observed in the GaSb/GaAs system [41]. However, the reverse group-V exchange reaction (As/Sb exchange), i.e., Sb segregation, also takes place upon capping of the Sb-containing layer [42-44]. The reduction in the CC growth temperature is likely to reduce in the As/Sb exchange between the corresponding InSb and InAs cap layer consequently reducing the segregation in the material. However, if segregation was the only phenomenon responsible for the Sb distribution observed, a thinner and Sb-rich layer would be expected in the sample with the InAs CC grown at the lowest temperature (310ºC). Instead, our 002 DF images show that the InSb layer in this structure is clearly thicker than those obtained with InAs caps grown at higher temperatures. Because of this, the authors think that Sb evaporation at higher temperatures should also be taking place, similarly to that proposed by Bennet *et. al* [40]. Thus, the decrease in the InAs CC growth temperature would produce a decrease in both the Sb segregation and the Sb evaporation during growth, leading from a layer with Sb-rich clusters to a more continuous InSb-rich layer. These changes in the InSb distribution in the material have shown to affect the PL emission of the material, exhibiting a clear red-shift due to the increase in the Sb content. A further reduction in the InAs CC growth temperature may help to increase the Sb incorporation in the layer, although care should be taken to maintain a high quality of the epitaxial growth to avoid possible structural imperfections observed at low growth temperatures [45]. Although the present work constitutes a step forward in the understanding of the growth process of SML InSb QDs, further work is needed to fully control the structural and functional properties of these promising nanostructures.
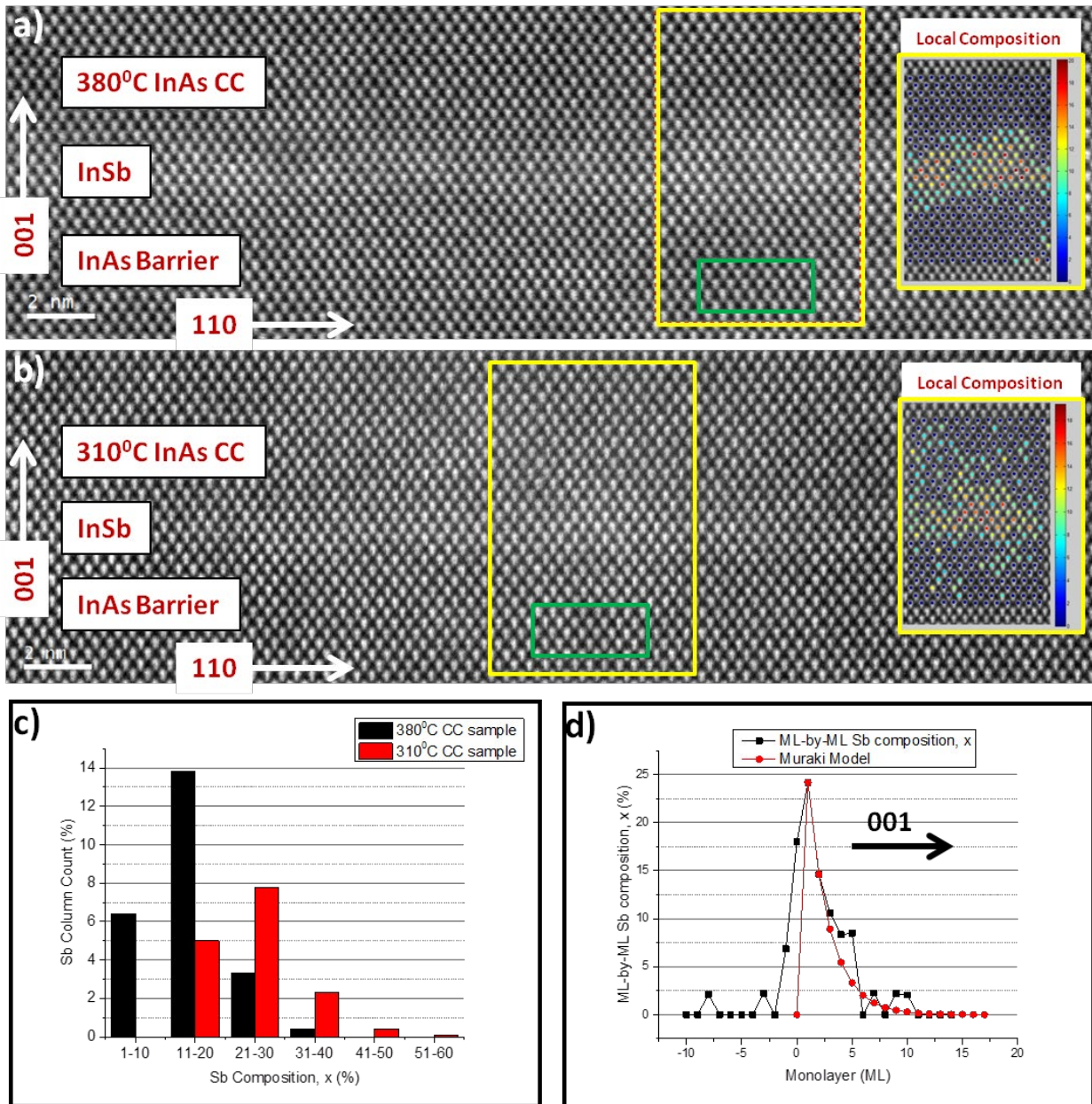
Figure 3: HAADF-(S)TEM images of single InAs/InSb/InAs layer associated with (a) 380ºC and (b) 310ºC InAs CC samples. The insets represent atomic column-by-column colored Sb composition maps (in %) generated within the respective yellow rectangles in those images. (c) A histogram exhibiting cumulative Sb atomic column counts (in %) for different Sb composition ranges in both CC samples. (d) ML-by-ML Sb average Sb composition (in black) along the [001] growth direction calculated from the Sb composition map in Figure 3b; the red curve represents the Muraki fit of the experimental data.

Conclusions

In summary, we have investigated the effect of including InAs CC grown at 380ºC and 310ºC in the SML deposition of InSb within InSb/InAs heterostructures grown by MEE. Our results by XRD and TEM have demonstrated that reducing the InAs cap growth temperature is an effective tool to increase the Sb

incorporation in SML InSb/InAs heterostructures during the epitaxial growth of the material. 002 DF images reveal random InSb agglomerates in the layers, that lead to a more continuous layer for the lower InAs CC growth temperature of 310ºC. The quantitative atomic column resolved HAADF-(S)TEM analysis reveals atomic columns with larger Sb composition when the InAs CC growth temperature is reduced. Our results show that the introduction of InAs CC is a plausible approach to control the Sb distribution by reducing As/Sb exchange and Sb evaporation in SML InSb/InAs heterostructures.

Acknowledgements

ORCID iDs

A A Khan: 0000-0002-0322-5024
E Repiso: 0000-0003-1895-7444
M Herrera: 0000-0002-2325-5941
P Carrington: 0000-0003-2107-5602
M de la Mata: 0000-0002-1581-4838
J Pizarro: 0000-0002-4295-6743
A Krier: 0000-0003-4098-5206
S I Molina: 0000-0002-5221-2852

References:

1. Kim Y, Kim J O and Lee S J 2018 Submonolayer quantum dots for optoelectronic devices *J. Korean Phys. Soc.* **73** 833-40
2. Xu Z, Birkedal D, Hvam J M, Zhao Z, Liu Y, Yang K, Kanjilal A and Sadowsky J (2003) Structure and optical anisotropy of vertically correlated submonolayer InAs/GaAs quantum dots *Appl. Phys. Lett.* **82** 3859
3. Stranski I N and Krastanow L 1938 Zur Theorie der orientierten Ausscheidung von Ionenkristallen aufeinander Abhandlungen der Mathematisch-Naturwissenschaftlichen Klasse IIb. *Akademie der Wissenschaften Wien* **146** 797-810
4. Asahi H 1997 Self-organized quantum wires and dots in III-V semiconductors *Adv. Mat.* **9** 1019-1026
5. Ivanov S V, Semenov A N, Solov'ev V A, Lyublinskaya O G, Terent'ev Y V, Mel'tser B Y, Prokopova L G, Sitnikova A A, Usikova A A, Toropov A A and Kop'ev P S 2005 Molecular beam epitaxy of type II InSb/InAs nanostructures with InSb sub-monolayers *J. Cryst. Grwth.* **278** 72-77
6. Carrington P J, Solov'ev V A, Zhuang Q, Ivanov S V and Krier A 2008 Type II InSb/InAs quantum dot structures grown by molecular beam epitaxy using Sb_2 and As_2 fluxes *Proc. of SPIE* **6900:** Quant. Sens. Nanophot. Dev. V 6900I
7. Solov'ev V A, Lyublinskaya O G, Semenov A N, Mel'tser B Y, Solnyshkov D D, Terent'ev Y V, Prokopova L A, Toropov A A, Ivanov S V and Kop'ev P S 2005 Room-temperature 3.9-4.3 μm

photoluminescence from InSb submonolayers grown by molecular beam epitaxy in an InAs matrix *Appl. Phys. Lett.* **86** 011109

8. Solov'ev V A, Sedova I V, Lyublinskaya O G, Semenov A N, Mel'tser B Y, Sorokin S V, Terent'ev Y V and Ivanov S V 2005 Midinfrared injection-pumped laser based on a III-V/II-VI hybrid heterostructure with submonolayer InSb insets *Tech. Phys. Lett.* **31** 235-37

9. Lyublinskaya O G, Solov'ev V A, Semenov A N, Mel'tser B Y, Terent'ev Y V, Prokopova L A, Toropov A A, Sitnikova A A, Rykhova O V and Ivanov S V 2006 Temperature-dependent photoluminescence from type-II InSb/InAs quantum dots *J. Appl. Phys.* **99** 093517

10. Mikhrin S S, Zhukov A E, Kovsh A R, Maleev N A, Ustinov V M, Shernyakov Y M, Soshnikov I P, Livshits D A, Tarasov I S, Bedarev D A, Volovik B V, Maximov M V, Tsatsul'nikov A F, Ledentsov N N, Kop'ev P S, Bimberg D and Alferov Z I 2000 0.94 μm diode lasers base on Stranski-Krastanow and sub-monolayer quantum dots *Semicond. Sci. Technol.* **15** 1061-64

11. Kim J O, Sengupta S, Barve A V, Sharma Y D and Adhikary S 2013 Multi-stack InAs/InGaAs sub-monolayer quantum dots infrared photodetectors *Appl. Phys. Lett.* **102** 011131

12. Hopfer F, Mutig A, Fiol G, Kuntz M, Shchukin V A, Haisler V A, Warming T, Stock E, Mikhrin S S, Krestnikov I L, Livshits D A, Kovsh A R, Bornholdt C, Lenz A, Eiesel H, Dähne M, Ledentsov N N and Bimberg D 2007 20 Gb/s 85^{0}C error-free operation of VCSELs based on submonolayer deposition of quantum dots *IEEE J. Top. Quant. Elect.* **13** 1302-08

13. Cirlin G, Petrov V and Dubrovskii V 1997 Direct formation of InGaAs/GaAs quantum dots during submonolayer epitaxies from molecular beams *Czech. J. Phys.* **47** 379-84

14. Horikoshi Y, Kawashima M and Yamaguchi H 1986 Low-temperature growth of GaAs and AlAs-GaAs quantum well layers by modified molecular beam epitaxy *Jap. J. Appl. Phys.* **25** L868-70

15. Germann T D, Strittmatter A, Pohl J, Pohl U W, Bimberg D, Rautiainen J, Guina M and Okhotnikov O G 2008 High-power semiconductor disk laser based on InAs/GaAs submonolayer quantum dots *Appl. Phys. Lett.* **92** 101123

16. Bressler-Hill V, Lorke A, Varma S, Petroff P M, Pond K and Weinberg W H 1994 Initial stages of InAs epitaxy on vicinal GaAs(001)-(2X4) *Phys. Rev. B* **50** 8479-87

17. Hopfer F, Mutig A, Kuntz M, Fiol G, Bimberg D, Ledentsov N N, Shchukin V A, Mikhrin S S, Livshits D L, Krestnikov I L, Kovsh A R, Zakharov N D and Werner P 2006 Single-mode submonolayer quantum-dot-vertical-cavity surface-emitting lasers with high modulation bandwidth *Appl. Phys. Lett.* **89** 141106

18. Sengupta S, Kim J O, Barve A V, Adhikary S, Sharma Y D, Gautam N, Lee S J, Noh S K, Chakrabarti S and Krishna S 2012 Sub-monolayer quantum dots in confinement enhanced dots-in-a-well heterostructure *Appl. Phys. Lett.* **100** 191111

19. Lam P, Wu J, Tang M, Jiang Q, Hatch S, Beanland R, Wilson J, Allison R and Liu H 2014 Submonolayer InGaAs/GaAs quantum dot solar cells *Sol. Ener. Mat. Sol. Cell* **126** 83-87

20. Carrington P J, Solov'ev V A, Zhuang Q, Krier A and Ivanov S V 2008 Room temperature midinfrared electroluminescence from InSb/InAs quantum dot light emitting diodes *Appl. Phys. Lett.* **93** 091101

21. Khan A A, Herrera M, Fernández-Delgado N, Reyes D F, Pizarro J, Repiso E, Krier A, Molina S I 2019 Investigation on Sb distribution for InSb/InAs sub-monolayer heterostructure using TEM techniques *Nanotech.* **31** 025706

22. Haugan H J, Brown G J and Peoples J A 2017 On the study of Sb incorporation in InAs/InAsSb superlattices for infrared sensing *J. Vac. Sci. Technol. B* **35** 02B107

23. Timm R, Lenz A, Eisele H, Ivanova L, Dähne M, Balakrishnan G, Huffaker D L, Farrer I and Ritchie D A 2008 Quantum ring formation and antimony segregation in GaSb/GaAs nanostructures *J. Vac. Sci. Technol. B* **26** 1492-1503

24. Hodgson P D, Bentley M, Delli E, Beanland R, Wagener M C, Botha J R and Carrington P J 2018 Optical and structural properties of InGaSb/GaAs quantum dots grown by molecular beam epitaxy *Semicond. Sci. Technol.* **33** 125021

25. Zhuang Q, Carrington P J and Krier A 2008 Growth optimization of self-organized InSb/InAs quantum dots *J. Phys. D: Appl. Phys.* **41** 232003

26. Malis T, Cheng S C and Egerton R F 1988 EELS log-ratio technique for specimen-thickness measurement in the TEM *J. Elect. Microsc. Tech.* **8** 193-200

27. Semenov A, Lyublinskaya O G, Solov'ev V A, Mel'tser B Y and Ivanov S V 2007 Surface segregation of Sb atoms during molecular-beam epitaxy of InSb quantum dots in an In(As)Sb matrix *J. Cryst. Grwth.* **301-302** 58-61

28. Ripalda J M, Alonso-Álvarez D, Alén B, Taboada A G, García J M, González Y and González L 2007 Enhancement of the room temperature luminescence of InAs quantum dots by GaSb capping *Appl. Phys. Lett.* **91** 012111

29. Guimard D, Tsukamoto S, Nishioka M and Arakawa Y 2006 1.55 µm emission from InAs/GaAs quantum dots by metal organic chemical vapor deposition via antimony incorporation *Appl. Phys. Lett.* **89** 083116

30. Fewster P F 1993 X-ray diffraction from low-dimensional structures *Semicond. Sci. Technol.* **8** 1915-34

31. Shen X-M, Li H, Liu S, Smith D J and Zhang Y-H 2013 Study of InAs/InAsSb type-II superlattices using high-resolution x-ray diffraction and cross-sectional electron microscopy *J. Cryst. Grwth.* **381** 1-5

32. Ngo C Y, Yoon S F, Fan W J and Chua S J 2006 Effects of size and shape on electronic states of quantum dots *Phys. Rev. B* **74** 245331

33. Jones L 2016 Quantitative ADF STEM: acquisition, analysis and interpretation *IOP Conf. Ser.: Mat. Sci. Engg.* **109** 012008

34. Molina S I, Sales D L, Galindo P L, Fuster D, González Y, Alén B, González L, Varela M and Pennycook S J 2009 Column-by-column compositional mapping by Z-contrast imaging *Ultramic.* **109** 172-76

35. Hernández-Maldonado D, Herrera M, Alonso-González P, González Y, González L, Gazquez J, Varela M, Pennycook S J, Guerrero-Lebrero M P, Pizarro J, Galindo P L and Molina S I 2011 Compositional analysis with atomic column spatial resolution by 5th-order aberration-corrected scanning transmission electron microscopy *Microsc. & Microanal.* **17** 578-81

36. Khan A A, Herrera M, Pizarro J, Galindo P L, Carrington P J, Fujita H, Krier A and Molina S I 2019 Modified qHAADF method for atomic column-by-column compositional quantification of semiconductor heterostructures *J. Mater. Sci.* **54** 3230-41

37. Muraki K, Fukatsu S, Shiraki Y and Ito R 1992 Surface segregation of In atoms during molecular beam epitaxy and its influence on the energy levels in InGaAs/GaAs quantum wells *Appl. Phys. Lett.* **61** 557-59

38. Lu J, Luna E, Aoki T, Steenbergen E H, Zhang Y H and Smith D J 2016 Evaluation of antimony segregation in InAs/InAs1-xSbx type-II superlattices grown by molecular beam epitaxy *J. Appl. Phys.* **119** 095702

39. Steinshnider J, Harper J, Weimer M, Lin C H, Pei S S and Chow D H 2000 Origin of antimony segregation in GaInSb/InAs strained-layer superlattices *Phys. Rev. Lett.* **85** 4562-65

40. Bennett B R, Shanabrook B V and Twigg M E 1999 Anion control in molecular beam epitaxy of mixed As/Sb III-V heterostructures *J. Appl. Phys.* **85** 2157-61

41. Hatami F, Ledentsov N N, Grundmann M, Böhrer J, Heinrichsdorff F, Beer M, Bimberg D, Ruvimov S S, Werner P, Gösele U, Heydenreich J, Richter U, Ivanov S V, Meltser B Y, Kop'ev P S and Alferov Z I 1995 Radiative recombination in type-II GaSb/GaAs quantum dots *Appl. Phys. Lett.* **67** 656-58

42. Xie Q, Nostrand J E V, Brown J L and Stutz C E 1999 Arsenic for antimony exchange on GaSb, its impact on surface morphology, and interface structure *J. Appl. Phys.* **86** 329-37

43. Nosho B Z, Bennett B R, Whitman L J and Goldenberg M 2001 Effects of As2 versus As4 on InAs/GaSb heterostructures: As-for-Sb exchange and film stability *J. Vac. Sci. Technol. B* **19** 1626-30

44. Brown T, Brown A and May G 2002 Anion exchange at the interfaces of mixed anion III-V heterostructures grown by molecular beam epitaxy *J. Vac. Sci. Technol. B* 20 1771-76

45. Ye H, Li L, Hinkey R T, Yang R Q, Mishima T D, Keay J C, Santos M B and Johnson M B 2013 MBE growth optimization on InAs (001) homoepitaxy *J. Vac. Sci. Technol. B* **31** 03C135